

# Gravity driven shallow granular flows down flat frictional channels

Nicolas Brodu, Patrick Richard, and Renaud Delannay

*Institut Physique de Rennes, Université de Rennes 1,*

*Campus de Beaulieu Bâtiment 11A, 263 av. Général Leclerc, 35042 Rennes CEDEX*

(Dated: December 22, 2011)

Granular flows down flat inclined channels are commonly used in the industry. In spite of their practical importance, they have not been investigated in details yet. Using DEM numerical simulations we find that stationary states occur for an unexpectedly large range of angles of inclination. We report previously unseen stationary regimes, with secondary rolls and with a supported dense slab on top of a granular gas. These are stabilized by the lateral boundaries at high angles.

*Introduction*— Granular dense flows down inclined channels are of interest in engineering applications involving conveying of solid materials such as minerals, or in geophysical situations like rock avalanches or pyroclastic blasts. They preserve the complexity of granular flows while remaining simple enough for a detailed analysis [1]. The solid boundaries are known to change the flow structure [2]. The choice of wide channels is an attempt to avoid the influence of sidewalls. In the same way numerical simulations in periodic cells attempt to study flows down infinitely long and wide chutes. When periodic boundaries are used in the direction of the flow, only steady fully developed (SFD) flows are meaningful. Attainment of SFD flows is nevertheless restricted in experiments by the physical length of the chute, as pointed out in [3]. Our simulation results below are a strong indication that many flows experimentally tagged as “accelerated” would in fact achieve SFD conditions with longer chutes. Periodic boundary conditions (PBC) offer the advantage of decreasing the number of free parameters. The same simplicity argument leads to characterize the overall behavior of grain interactions through material parameters such as restitution or friction coefficients. Even with such simple choices: flat frictional base, PBC in both flow and vorticity directions and description of interactions between spherical beads and with the base through identical coefficients, there remains at least 9 “parameters” [4] that can influence the numerical simulation of the channel flow. Walton [5] performed numerical simulations using these simple conditions. He showed that SFD flows develop only for inclination angles  $\theta$  whose tangent is smaller than the friction coefficient  $\mu$ , else they accelerate unboundedly. Louge and Keast [6] conducted experiments on flat base with a well documented set of parameters; we use them as input for our numerical simulations. Introducing side walls in the simulation allows us to recover characteristics more compatible with the experiments and reveals their relatively long-range influence. At larger angles we show the presence of an internal structure: secondary rolls, turning into a “supported regime” as  $\theta$  increases, whereby an agitated granular layer forms at the base. These SFD flows appear even for large angles  $\theta \gg \text{atan}\mu$ , so they cannot be captured by PBC in the vorticity direction on a flat

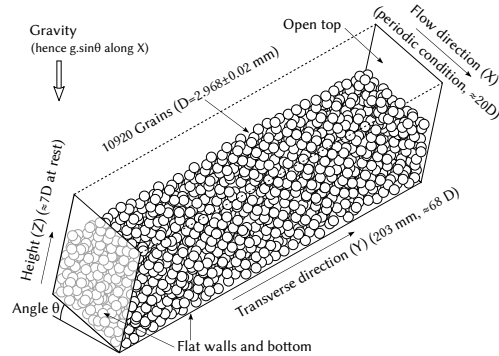


FIG. 1. Sketch of the MD simulation in a configuration corresponding to experiments [6] where an inclined plane is bounded by flat side walls and bottom.

base. To our best knowledge, our work is the first to report that secondary flows also exist with flat boundaries. The only evidence of rolls and supported regimes were reported for accelerated flows and bumpy boundary conditions [2, 7–9]. We thus show that these rolls are a generic feature inherent to the granular flows dynamic present for a large class of boundary conditions. Stationary states in these conditions are not easy to achieve in laboratory, despite their likely occurrence in nature and industry. In this paper, we explore how this new regime is affected by geometry and granular parameters.

*Simulation method and PBC results*— We perform 3D numerical simulations of granular flows using molecular dynamics (MD). Grains are modeled as overlapping non-deformable spheres by means of a spring and dash-pot combination for both the normal and the tangential directions, with static friction [9–11]. The simulations are carried out for a fixed number of slightly polydisperse spheres. The calculational space is bounded on the bottom by the fixed flat frictional XY plane, it is free on the top surface (see Fig. 1). PBC are applied in the flow (X) direction and, only for the first simulations, in the Y direction. The system is bound by side walls whose properties are the same as the base. We also performed some simulations with bumpy surfaces made of glued grains having the same material properties as the flat boundaries.

The simulation setup (Fig. 1) is designed to match the experimental setup of Louge and Keast [6], with minor adaptations. We used the same bead size and polydispersity, the geometry is the same except for PBC along

X. Initial conditions consist of dropping a loose assembly of grains at a small altitude, with some agitation. These low energy initial conditions and the mass holdup we use [12] are compatible with those observed experimentally for all SFD flows in [6]. Coefficients of restitution have the experimental values given in [6, 13]:  $e_{gg}^n = 0.973$  and  $e_{gw}^n = 0.8$  for the normal components, and  $e_{gg}^t = 0.25$ ,  $e_{gw}^t = 0.35$  for the tangential components, where the subscripts  $gg$  and  $gw$  denote, respectively, impacts between two grains and between a grain and a wall. The model normal springs stiffness is  $k_{gg}^n = k_{gw}^n = 3.10^5 \text{N/m}$  and tangential values  $k^t$  deduced from  $k^n$  [10]. These values are comparable to other simulations using realistic material properties ( $k^n = 2.10^5 \text{N/m}$  in [3]). The static friction coefficient  $\mu_{gw} = 0.593$  is mentioned in [6] but not the value of  $\mu_{gg}$ . Measurements in our lab give  $\mu_{gg} = 0.33$  for similar glass beads.

Preliminary simulations using periodic boundary conditions along Y were performed with the above friction and restitution coefficient values. These resulted in steady flows for angular ranges that do not match the experimental results from [6], with  $\theta_{\min} \approx 6 - 7^\circ$  and  $\theta_{\max} \approx 24^\circ < \text{atan}\mu_{gw}$ . We tried other values of the friction coefficients, changed the polydispersity and introduced other sources of dissipation (rolling friction [11]) but  $\theta_{\min}$  remains always small compared to the experimental value. We thus perform all other simulations with side walls, which introduce additional friction able to increase  $\theta_{\min}$ .

*Results with side walls*— We ran systematic simulations for a range of angles from  $12^\circ$  to  $33^\circ$  every half degree. Fig. 2a presents the evolution of the kinetic energies of the flow over time. For  $\theta \leq 13.5^\circ$  we observe low velocity flows with large fluctuations. Arrest is difficult to obtain with nearly monodisperse spherical beads rolling on flat base. These flows (zones marked A in Fig. 2) are stopped in additional simulations using a higher polydispersity. We suspect that they match jammed states in experiments (e.g. due to dust between grains [13] or non-sphericity). For  $\theta \geq 13.5^\circ$ , the flows reach after some time a steady (B,D,E) or an oscillating (C) state. We define the time and distance necessary to converge towards the limit steady state, as determined by both translational and rotational kinetic energy levels being within 5% of their final average levels. They are shown in Fig. 2a with markers. Results presenting time average quantities (e.g. velocity, packing fraction) are computed starting from that time. Fig. 2b (resp. 2c) represents the velocity profile averaged along Z (resp. Y) as a function of Y (resp. of Z), for each value of inclination angle.

These profiles and the color-coded packing fraction in Fig. 2c allow us to identify the following regimes:

— Unidirectional SFD flows: In the zones marked B on Fig. 2:  $\theta \in [13.5^\circ, 17.5^\circ]$ , grains are forming “crystallized” blocks moving along X in average. These blocks

also appear in Fig. 2c as regions of higher packing fraction. They imposed some averaging over multiple runs to smooth them out. Simulations were also performed with higher-energy initial conditions, which resulted in qualitatively the same phase diagram except with less inter-run variability.

— Oscillating flows: In the zones marked C,  $\theta \in [17.5^\circ, 19.5^\circ]$ , the aforementioned blocks have “melted” and the flow presents some agitation, as well as a few grains jumping over the surface. Relatively large fluctuations are visible on the translation and rotation kinetic energies at  $\theta = 19^\circ$  (Fig. 2a).

— Secondary SFD flows (rolls): this regime (marked D:  $\theta \in [19.5^\circ, \approx 28^\circ]$ ) corresponds to the advent of secondary flows (Fig. 2b, insert). As visible on Figs. 2c and 2b (insert), typical flow heights vary between 10 and 15 grain diameters within phase D. Since there are 68 grain diameters in the transverse (Y) direction the rolls are quite flat. The packing fraction  $\nu \approx 0.4$  decreases slightly with  $\theta$  but remains almost constant through the height. The velocity profile (Fig. 2b) is sheared through the whole width, even in the conditions of the experiment where the base width is about ten times the flow height at rest (Fig. 3e).

— SFD flows supported by a granular gas basal layer: Fig. 2c, zone marked E, shows a fast-moving slab of high packing fraction supported by a low-density zone. There is no clear surface but a dilute granular gas top reaches far larger heights (Fig. 2c, logarithmic scale) than in the previous regimes. The end of the phase D is clearly apparent on the profiles in Fig. 2b but the transition between D and E is progressive over a range of angles ( $27^\circ \leq \theta \leq 29^\circ$ ) according to the packing fraction profile in Fig. 2c. The density averaged on a transverse section shown in Fig. 3 reveals that the dense core ( $\nu \approx 0.5$ ) is supported on both walls and bottom. The internal structure of the supported slab (Fig. 3d) is reminiscent of the rolls. As the angle increases the dense core slowly vanishes into a purely gaseous regime, at surprisingly high angle values ( $\approx 60^\circ$ ) given the low mass holdup and large width of our setup.

Simulations with sidewalls lead to SFD flows even for angles much larger than  $\text{atan}\mu_{gw}$  (tested up to  $70^\circ$ ). As for SSH [14], in order to maintain its steady state for large values of  $\theta$  the flow has to adapt its height to increase the contact surface and the pressure on the walls, which can be seen clearly in Fig. 2c. We see on Fig. 3e that  $\tan\theta$  varies linearly with the height  $H$  of the flow in the supported regime and at the end of the rolls regime D, with a clear transition between them. We checked that the pressure on the walls varies roughly linearly with depth, we can thus apply the same reasoning as in [14] and obtain  $\mu_B + \frac{H}{W}\mu_W = \tan\theta$ , with  $\mu_B$  and  $\mu_W$  effective global friction coefficients on the bottom and the walls. Interestingly  $\mu_B$  and  $\mu_W$  are both smaller than  $\mu_{gw}$ , but surprisingly  $\mu_B$  is smaller in regime D than

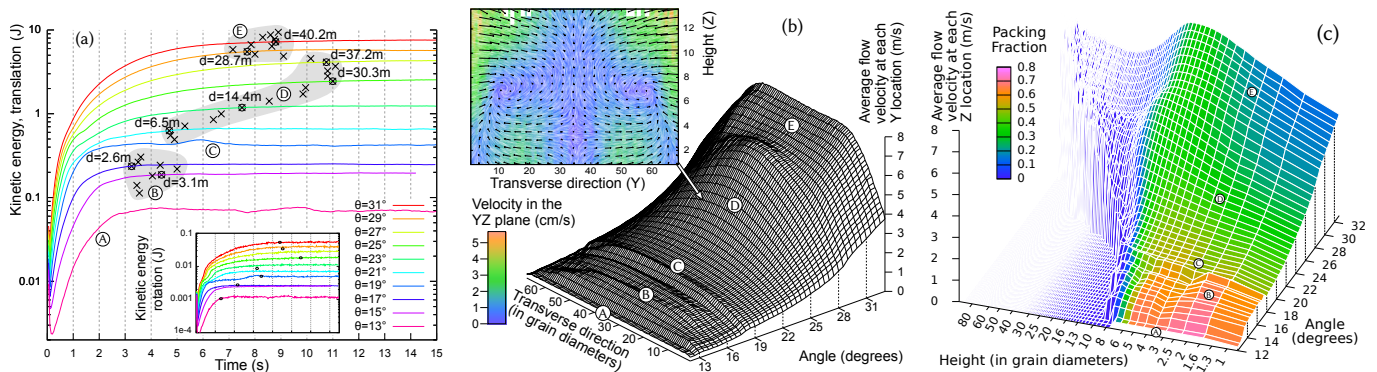


FIG. 2. Phase diagrams showing the characteristics of the SFD flow regimes, in the range  $\theta \in [12 \dots 33]$ . (a) Translation and rotation (insert) kinetic energies vs time, and distances before reaching the steady state. (b) Secondary flow (insert, color-coded velocity in the YZ plane) and transverse velocity profile of the different phases. (c) Height velocity profile vs angle, packing fraction (color-coded).

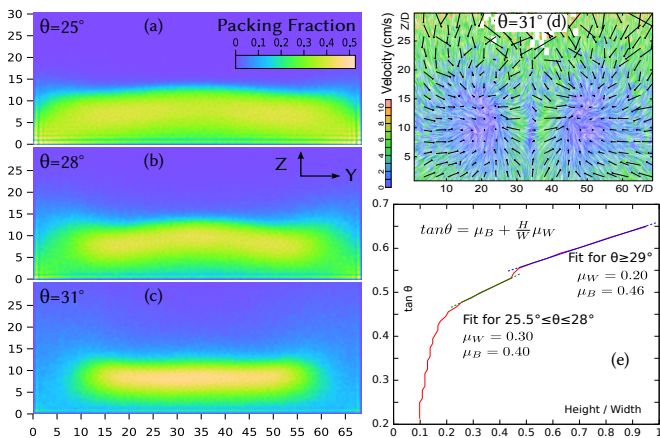


FIG. 3. Transition to supported flows. (a-c) Cross-section average of the packing fraction for 3 angles at the transition. (d) Internal structure of the supported slab ( $\theta = 31^\circ$ ). (e) Tangent of the inclination angle plotted as a function of  $H/W$ .  $H$  is set to the height at which the pressure is 0.5% of the average pressure value  $P_B$  on the bottom.

in the supported regime E. Complementary simulations show that values of  $\mu_B$  and  $\mu_W$  depend on the configuration parameters, like  $W$  and the mass holdup. These simulations also reveal that walls can be separated wide apart without collapse of the supported slab (tested up to  $W=30H$ ).

*Discussion*— Oscillations were reported experimentally in [6]. Hanes and Walton [3], who use a bumpy base for their experiments, also report a phase diagram with an oscillating regime delimited by fuzzy boundaries, at the junction of two SFD regimes. In their simulations using PBC along the flow, they observed temporal oscillations which could be a manifestation of these surging flows. Visual investigation of the simulations as well as rotation velocity profiles along  $Z$  show that the flows in the B-C zones consist of a plug sliding on top of a basal

layer of grains, for which there is a combination of long-lasting rolling contacts on the smooth bottom interrupted by short rebounds. Louge and Keast [6] experimentally observed a range of angles for steady states from  $15.5^\circ$  to  $20^\circ$ , established over distances less than 3m. This matches our regime B ( $13.5^\circ \leq \theta \leq 17.5^\circ$ ,  $d \approx 3m$ , Fig. 2a) and probably the oscillating flows C. Values of the packing fraction at the base of the flow (Fig. 2c) are also compatible with the experiments (Fig. 6 of [6]). Fig. 3e also shows that in the range of angles corresponding to the B-C regimes, aspect ratios keep a low value. This is consistent with [6] finding an aspect ratio  $\frac{H}{W} < 0.17$  and thus a negligible influence of the friction on the side walls. At the center of the flow we obtain vertical velocity profiles similar to these given by PBC [5]. Nevertheless, Fig. 2b reproduces in the B-C zones the experimental velocity transverse profile (Fig. 7 of [6]), where the shearing layer induced by the walls extends to about  $1/3$  within the flow. Hence the role of boundary conditions is not limited to friction but more complicated effects come into play (e.g. frustration of rotations).

When the inclination increases, our simulations predict the appearance of secondary rolls which lift up to give birth to a supported regime. The supported regime appears here with smooth bottom and walls, but we checked that the regime E also exists in the presence of rough boundaries made of glued grains. Numerical simulations with PBC along  $Y$  and a rough base [9] can exhibit a “stripes dense” and a “stripes dilute” regimes, similar to our regimes D and E respectively, although these appear only up to a limit angle of  $39^\circ$  in these conditions. The flow initiates an expansion at the base, but fails to stabilize at large angles as it has no frictional surface to expand on. On a flat base the supported regime E only exists when the walls are present. The main limiting factor for observing regimes D and E experimentally is the distance necessary for the steady state to take place: about 30m for the supported phase when starting with

little initial energy and for grains about 3mm diameter. It is thus not surprising that over the first few meters the corresponding configurations were interpreted experimentally as accelerated or unstable: rolls were reported in experiments with rough glued grain boundaries in accelerated flows [7, 8]. Nevertheless the additional phases are accessible experimentally by reducing the diameter of the grains and/or by giving them some initial velocity. Secondary flows have been observed in experiments within a rough channel [2] (using 0.5mm beads) and [9] ( $D=0.4\text{mm}$ ). The stationary state in [2] was reached at a distance compatible with our results: less than 3m at  $\theta = 23.6^\circ$ . The average packing fraction at the transition between D and E regimes is about 0.3. It is compatible with the values observed in [9] for the transition between dense and dilute stripes. The secondary SFD flows could also correspond to the steady collisional phase observed in [3] for flows between flat walls, but on a rough base. The supported layer is reminiscent of the density inversion on a bumpy bottom mentioned in [15] except that in [15] it exists only for a specific value of the angle and high-energy initial conditions. In our case the supported regime is obtained for a large range of angles and appears naturally as an extension of the previous phases.

The transitions between the regimes and their characteristics depend on the model parameters (e.g. friction coefficients, polydispersity of the grains) but some of the general features of the flows seem robust. For instance, additional runs with  $\mu_{gg} = 0.4$  instead of 0.33 shifted the start and end of phase B up by  $1^\circ$ . The crystallized blocks in the unidirectional SFD flows (B) do not appear when using more polydisperse grains, but the oscillations (C) are still present. The rolls (D) and supported slab (E) are robust to polydispersity (tested with  $D \pm 20\%$ ). They also appear when  $\mu_{gg} = \mu_{gw}$  (customary setup in numerical works [10]), provided both are greater to about 0.54. Additional simulations showed that gluing grains on the boundaries prevents the rolls but induce a large internal agitation instead, consistently with Fig. 3d of [9] where rolls have been reported on rough bottom only with larger channels and thicker flows.

We also varied the mass holdup so as to match the range of shallow flow configurations in [6]: low  $H^\dagger = 1$  induces an early transition to the gaseous phase without secondary flows. The regimes (D,E) also exist for  $H^\dagger = 7$ .

*Conclusion*— We find SFD flows corresponding to the experimental setup [6] with compatible range of angles, distances of establishment and velocity profiles. Building on these results we predict the existence of additional phases for the flows bounded by flat boundaries at high angles: secondary rolls, turning into a supported dense slab atop a layer of granular gas. We have shown that these are robust generic features of granular flows, extending previous experimental and numerical studies [7, 9, 10] to flat boundaries and to SFD flows at higher angles, owing to stabilization by the walls. The secondary

rolls occur on a flat surface even for a small number of layers of grains.

Even if the distance necessary for the predicted phases to take place is relatively long, they probably appear in a wide range of industrial and natural contexts, for example when sand is transported in conduits over a moderate distance ( $\approx 5\text{m}$ , scaling our results down for  $500\mu\text{m}$  grains). Effects similar to the supporting granular gas layer may also be at work for long runout landslides and avalanches. This part of the phase diagram with higher mass holdups  $H^\dagger$ , in relation with the observed reduction of effective friction on solid boundaries in our numerical simulations, requires more investigation and will be the topic of future works.

Flows down inclined channels exhibit a rich flow structure with a simple setup, which is ideal for studying granular theories. The flat walls geometry seems to induce a faster convergence to the steady states than PBC in the vorticity direction, while presenting the same flow structures. It is thus better adapted for testing granular rheologies and how they deal with boundary conditions, especially since channelled flows can be directly compared to experiments while PBC are, by essence, non-physical.

*Acknowledgments*— We thank Région Bretagne for funding (CREATE Sampleo Grant) and M.Y.Louge and J.T.Jenkins for helpful discussions and comments.

- 
- [1] R. Delannay, M. Louge, P. Richard, N. Taberlet, and A. Valance, *Nature Mater.* **6**, 99 (2007).
  - [2] S. B. Savage, *J. Fluid Mech.* **92**, 53 (1979).
  - [3] D. M. Hanes and O. R. Walton, *Powder Tech.* **109**, 133 (2000).
  - [4] number of grains, their size distribution, initial positions and velocities, contact model with 3 material parameters, inclination angle.
  - [5] O. R. Walton, *Mech. of Mater.* **16**, 239 (1993).
  - [6] M. Y. Louge and S. C. Keast, *Phys. Fluids* **13**(5), 1213 (2001).
  - [7] Y. Forterre and O. Pouliquen, *J. Fluid Mech.* **486**, 21 (2003).
  - [8] T. Börzsönyi and R. E. Ecke, *Phys. Rev. E* **74**, 061301 (2006).
  - [9] T. Börzsönyi, R. E. Ecke, and J. N. McElwaine, *Phys. Rev. Lett.* **103**, 178302 (2009).
  - [10] L. E. Silbert, D. Ertas, G. S. Grest, T. C. Halsey, D. Levine, and S. J. Plimpton, *Phys. Rev. E* **64**, 051302 (2001).
  - [11] S. Luding, *Eur. J. Env. Civil Eng.* **12**, 785 (2008).
  - [12]  $H^\dagger = \int_0^{+\infty} \frac{\nu(z)}{D} dz = 4.14$  quantifies the amount of matter above a surface unit, with  $\nu$  the volume fraction.
  - [13] A. Lorenz, C. Tuozzolo, and M. Y. Louge, *Exp. Mech.* **37**, 292 (1997).
  - [14] N. Taberlet, P. Richard, A. Valance, W. Losert, J. M. Pasini, J. T. Jenkins, and R. Delannay, *Phys. Rev. Lett.* **91**, 264301 (2003).
  - [15] N. Taberlet, P. Richard, J. T. Jenkins, and R. Delannay, *Eur. Phys. J. E* **22** (2007).